Diffusional Anisotropy of Simple Sorbates in Silicalite

Sudeshna Kar and Charusita Chakravarty*

Department of Chemistry, Indian Institute of Technology-Delhi, Hauz Khas, New Delhi 110016, India

Received: October 20, 2000; In Final Form: March 12, 2001

Microcanonical ensemble molecular dynamics simulations are used to study anisotropy in diffusional and related dynamical properties for five spherical sorbates of varying size and polarizability in silicalite. Silicalite has straight and zigzag channels, parallel to the *y* and *x*-axes of the unit cell, respectively, which are interconnected in such a way that diffusion along the *z* direction is possible only by alternation of the sorbate between straight and zigzag channel segments. Helium, the smallest and most weakly bound sorbate, is found to comply most closely with the behavior expected on the basis of the simple random walk model developed to understand the geometrical correlation between the principal elements of the diffusional tensor in silicalite (J. Kärger, *J. Phys. Chem.* **1991**, *95*, 5558). The larger and more strongly bound sorbates, Ne, Ar, CH_4, and Xe, show significant deviations from this model. The diffusion of these particles along the *z* direction is distinctly subdiffusional with the mean square displacement growing as $\approx t^{0.8}$. The randomization and anisotropy parameters for all four sorbates are similar but differ significantly from the predictions of the random walk model. The relative rates of diffusion along the straight and zigzag channels are more sensitive to the nature of the sorbate than the anisotropy and randomization parameters. For all five sorbates, the subdiffusional behavior along the *z* direction, as well as deviations from the predictions of the random walk model, are more pronounced at higher concentrations. The anisotropy in the short-time dynamics has been examined by studying the velocity autocorrelation functions and the instantaneous normal mode spectra. For very short times of less than 0.5 ps, the velocity autocorrelation function and its directional analogues are virtually identical, but divergences are seen by times of the order of 1 ps. The instantaneous normal mode spectra show the expected correlation between the diffusion coefficient, the Einstein frequency, and the fraction of imaginary modes. There is no significant anisotropy in the INM spectra that is consistent with the behavior of the velocity autocorrelation functions for short time scales.

1. Introduction

Transport properties of simple sorbates in zeolites provide convenient models for understanding the effect of confinement in a microporous medium on the dynamics of fluids. Zeolites are ordered porous media with well-characterized crystallographic structures which provide a very wide variety of pore dimensions, binding energies, and channel geometries.[1−5] One of the most obvious ways in which confinement in a zeolite can alter the dynamics of a fluid is by inducing diffusional anisotropy due to a framework geometry belonging to a noncubic space group.[6−10] Other examples of unusual diffusional phenomena due to the structure of the confining medium are single file diffusion,[11−15] the levitation effect,[16−19] and quantum sieving.[20]

Silicalite is the pure silica analogue of the industrially important zeolite ZSM-5. Silicalite belongs to the orthorhombic *Pnma* space group and is therefore expected to induce diffusional anisotropy. Silicalite also has a more unusual feature in the geometry of the channel network that has made it the focus of a number of theoretical studies. Silicalite contains two types of interconnected channels: straight channels parallel to the *y* direction and zigzag channels parallel to the *x* direction. The channel connectivity is such that at a channel intersection the sorbate can move in one of the four directions in the *x*, *y*-channel system, and sorbate diffusion along the *z* direction is only possible by alternation of the sorbate between straight and zigzag channels. Thus diffusion in the *z* direction must depend on the diffusion coefficients in the *x* and *y* directions. This type of correlation between the components of the diffusion tensor due to the geometry of the channel network is classed as geometrical correlation. To understand the effect of such geometrical correlations on the diffusional anisotropy, Kärger developed a simple and elegant Markovian random walk model for diffusion in silicalite that predicts the following relationship between the diffusion coefficients, D_x, D_y, and D_z, in the *x*, *y*, and *z* directions:[6]

$$\frac{c^2}{D_z} = \frac{a^2}{D_x} + \frac{b^2}{D_y} \tag{1}$$

where *a*, *b*, and *c* are the unit cell dimensions. More elaborate models that take into account other sources of correlations, such as vacancy correlations due to concentrations significantly greater than zero and kinetic correlations due to incomplete randomization, have subsequently been developed.[9,10] For xenon, methane, and ethane, comparison of predictions based on random walk methods with pulsed field gradient NMR and molecular dynamics (MD) results indicate a fair degree of consistency.

In this work, we examine the diffusional anisotropy exhibited by simple Lennard−Jones sorbates in zeolites using molecular

* To whom correspondence should be addressed.

10.1021/jp0038658 CCC: $20.00
Published on Web 05/25/2001

TABLE 1: Lennard−Jones Parameters for the Sorbate−Sorbate and Sorbate−Oxygen Interactions

sorbate	ϵ_{SS} (kJ mol^{-1})	σ_{SS} (Å)	ϵ_{OS} (kJ mol^{-1})	σ_{OS} (Å)
He	0.085	2.28	0.426	2.62
Ne	0.28	2.85	0.529	2.78
Ar	1.183	3.35	1.028	3.03
CH_4	1.23	3.73	1.108	3.214
Xe	3.437	3.85	1.737	3.28

dynamics simulations. The dependence of the extent of anisotropy on sorbate size and polarizability is illustrated using Lennard−Jones parametrizations for helium, neon, argon, methane, and xenon. In addition to calculating the diagonal elements of the diffusion tensor, we also examine the anisotropy in several related quantities such as the velocity autocorrelation function and the ballistic to diffusional crossover times. Instantaneous normal mode (INM) analysis has been recently shown to be very useful for understanding short-time dynamical behavior of sorbates in zeolites.[21−23,25−27] For example, the INM spectrum carries signatures of the anomalous levitation peak. In this work, INM analysis is extended to study diffusional behavior in anisotropic zeolites. The paper is organized as follows. Simulation details and related techniques of analysis are summarized in Section 2. Results are discussed in Section 3. Conclusions are presented in Section 4.

2. Details of Simulations and Analysis

2.1 Zeolite Structure. The unit cell of silicalite contains 96 silicon atoms and 196 oxygen atoms. The positions of the framework atoms were taken from the crystallographic data for the orthorhombic form.[28,29] Silicalite belongs to the *Pnma* space group and has lattice parameters of $a = 20.07$ Å, $b = 19.92$ Å, and $c = 13.42$ Å. The straight channels parallel to the *y*-axis have elliptical cross sections, with major and minor axes of 5.7 and 5.1 Å, respectively, and are bisected by the planes $x = 0$ and $x = a/2$. The zigzag channels parallel to the *x*-axis with a circular cross section of 5.4 Å radius can be clearly seen in the planes $y = b/4$ and $y = 3b/4$.

2.2 Potential Energy Surface. The potential energy function for Lennard−Jones sorbates in silicalite is based on the Kiselev model.[30−32] The total potential energy of the system is subdivided into a guest−host term, U_{gh}, which represents the interaction between the sorbate or guest atom with the host lattice and a guest−guest term, U_{gg}, which is a pairwise Lennard−Jones interaction between the sorbate atoms. The silicon atoms in the framework are assumed to be completely shielded from interaction with the sorbate by the tetrahedrally coordinated oxygen atoms. Since silicalite contains no framework cations, it is not necessary to postulate compensating partial charges on the framework oxygens, and the only contribution to the guest−host interaction energy is due to the dispersion interaction between the sorbate and the framework oxygens. The functional form of the potential is then given by:

$$U_{gh} = \sum_{j=1}^{n_O}\sum_{i=1}^{N} 4\epsilon_{OS}\left(\frac{\sigma_{OS}^{12}}{r_{ij}^{12}} - \frac{\sigma_{OS}^{6}}{r_{ij}^{6}}\right) \qquad (2)$$

where n_O and N are the number of framework oxygen and sorbate atoms respectively, r_{ij} is the distance between the *j*th framework oxygen and the *i*th sorbate atom and ϵ_{SO} and σ_{SO} are the Lennard−Jones parameters for the sorbate−oxygen interaction. Table 1 shows the Lennard−Jones parameters for the sorbate−sorbate as well asorbate−framework oxygen interaction used in this work. Parameters for neon, argon, and xenon are taken from ref 33. The methane parameters are those used in a recent study of diffusional anisotropy.[8] The parameters for helium are taken from ref 24. Note that CH_4 has a very similar ϵ_{SS} value to Ar and a very similar σ_{SS} value to that of Xe. Figure 1 shows contour plots of the potential energy as a function of the location of a single rare gas atom in the silicalite framework. The steeper repulsive walls and reduced dimensions of the channels for the larger xenon atom when compared to helium are obvious. In the case of helium, additional very small pores can be seen that are isolated from the channel system and are artifacts of the potential energy surface. These unphysical pore spaces arise because the approximation of assuming complete shielding of the sorbate from direct interaction with framework silicon atoms breaks down when the sorbate size is small. The effect is small for helium, and the MD dynamics is not affected provided the simulation is initiated with the sorbates located in the channel regions. For very small sorbate sizes, however, the distortion of the channel geometry is substantial. In previous work on the levitation effect in silicalite, sorbates with Lennard−Jones size parameters as small as 1.5 Å were considered.[19] Our analysis of contour plots of such small sorbates indicates that the channel structure of silicalite is severely distorted in such cases, and we have therefore not considered any sorbates with σ_{SS} less than 2.28 Å in this study.

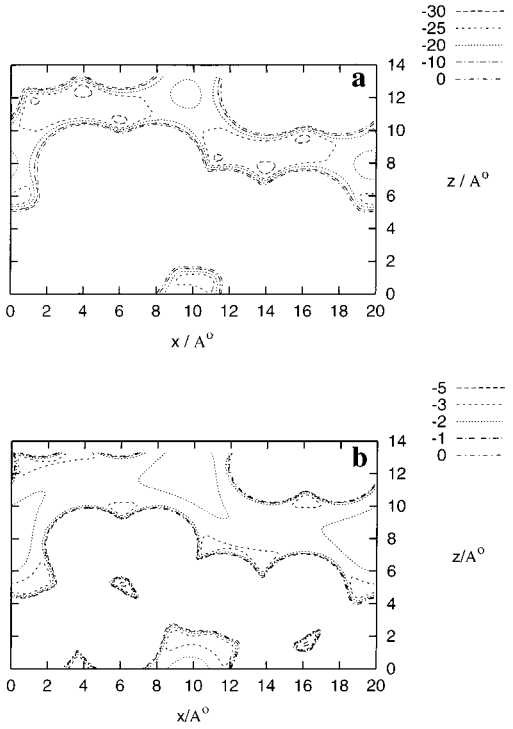

Figure 1. Contour plots of the potential energy surface of a single (a) xenon and (b) helium atom in silicalite. The plots are constructed in the *xz*-plane with *y*-coordinate fixed at 4.98 Å. Contour lines give the potential energy in kJ mol^{-1}.

2.3 Molecular Dynamics. *2.3.1 Computational Details.* Molecular Dynamics (MD) simulations were carried out in the microcanonical (NVE) ensemble using the velocity Verlet algorithm.[34,35] The simulation program developed by us has been tested against results available in the literature and used in previous work.[26,27] Initial velocities were sampled from a Maxwell−Boltzmann distribution corresponding to some preset temperature and then temperature scaling was carried out during the equilibration period. The reference temperature was taken

to be 300 K; actual temperatures during a run were within ±20 K of this value. Concentrations ranging from 2 to 24 sorbates per unit cell were studied. Orthorhombic periodic boundary conditions were imposed. A simulation cell containing two unit cells of silicalite along the *z*-axis in conjunction with a spherical cutoff radius of 12 Å for sorbate−sorbate and sorbate−zeolite interactions was found to be sufficient to converge the guest−host potential energy to better than 2%.[26,27] The zeolite framework was assumed to be rigid. The time step for each system was chosen to ensure energy conservation to better than the third significant figure. Instantaneous normal modes were calculated at intervals of 100 time steps. Further convergence details and choice of time steps, run lengths, and equilibration periods are discussed in Section 2.3.4.

It is useful to consider at this stage the possible implications with regard to our simulation results of the choice of a rigid, as opposed to a flexible, zeolite lattice. Previous studies comparing diffusional behavior of methane in rigid and flexible zeolite frameworks indicate that the inclusion of lattice vibrations has a relatively small effect on diffusion constants.[36−38] The reason for this is that the force constants for the zeolite framework bonds are very large, and as a result, the zeolite lattice vibrations are relatively weakly coupled to the sorbate motion. While the presence of lattice vibrations assists the equilibration process in the NVE ensemble simulations, it is by no means essential provided equilibration times are sufficiently long.[39] Moreover, our primary interest in this work is the effect of channel geometry and connectivity on the diffusional behavior of sorbates. In this context, we cite several recent works on the effect of geometrical correlations on diffusional behavior in silicalite[6−10] as well as on single-file diffusion,[11−15] which use the rigid lattice assumption. Therefore, we feel that for an exploratory study of the type presented in this work, the rigid lattice approximation is adequate provided appropriate care is taken with regard to equilibration. To ensure the latter, we have followed an equilibration protocol in which the system is first thermalized at a high temperature of 500 K and then cooled to 300 K in steps of 50 K, ensuring thermalization at intermediate temperatures.

2.3.2 Diffusion Coefficients. The mean squared displacement (MSD), $\Delta^2\boldsymbol{r}(t)$, may be defined as

$$\Delta^2\boldsymbol{r}(t) = \langle|\boldsymbol{r}_i(t) - \boldsymbol{r}_i(0)|^2\rangle \tag{3}$$

$$= 1/N \sum_{i=1}^{N} \frac{1}{(t_{max} - t)} \int_0^{t_{max}-t} [\boldsymbol{r}_i(t+\tau) - \boldsymbol{r}_i(\tau)]^2 d\tau \tag{4}$$

where t_{max} is the duration of the simulation. A plot of the mean-squared displacement, $\Delta^2\boldsymbol{r}(t)$, versus time, t, can be subdivided into two distinct regimes: (i) the initial ballistic regime for which $\Delta^2\boldsymbol{r}(t) \propto t^2$ and (ii) the diffusional regime with $\Delta^2\boldsymbol{r}(t)t$.[36] The Einstein relation in the diffusional regime defines the diffusion coefficient, D, to be

$$\langle|\boldsymbol{r}(t) - \boldsymbol{r}(0)|^2\rangle = 6Dt \tag{5}$$

where $\boldsymbol{r}(t)$ is the $3N$-dimensional position vector for the sorbate atoms at time t. The direction-dependent diffusion coefficient in the x direction, D_x, is defined as

$$\Delta^2\boldsymbol{x}(t) = \langle|\boldsymbol{x}(t) - \boldsymbol{x}(0)|^2\rangle = 2D_x t \tag{6}$$

where $\boldsymbol{x}$ is an N-dimensional vector. The definitions of D_x and D_y are analogous. In all the cases studied here, the time period until approximately 1 ps can be definitely classed as in the ballistic regime while beyond 10 ps, the system may be classed as in the diffusional regime. A least-squares fitting procedure was used to obtain straight line fits in the two regions using the expression:

$$\ln\langle|\boldsymbol{x}(t) - \boldsymbol{x}(0)|^2\rangle = \ln(2D_x) + n_x \ln t \tag{7}$$

and its analogues in the y and z directions. The three-dimensional generalization is

$$\ln\langle|\boldsymbol{r}(t) - \boldsymbol{r}(0)|^2\rangle = \ln(6D) + n \ln t \tag{8}$$

Ideally, the values of n_x, n_y, n_z, and n should be 2 and 1 in the ballistic and diffusional regions, respectively, but in practice deviations from integer power dependence are observed due to the effects of the confining potential.[36] Since such deviations from unity contain interesting information on the degree of subdiffusional character, we have used eqs 7 and 8 to fit our data rather than eqs 5 and 6 which enforce a linear dependence on time. The intercept of the plot of $\ln|\boldsymbol{x}(t) - \boldsymbol{x}(0)|^2$ against $\ln t$ is taken to be $2D_x$ in the one-dimensional case and $6D$ in the three-dimensional case. An order-N algorithm was used to compute the mean-square displacement as a function of time.[35] The ballistic to diffusional crossover time, τ_c, is taken to be the point of intersection of the straight line fits to the data in the ballistic and diffusional regimes.

Since the purpose of this study is to study diffusional anisotropy in silicalite, we summarize the different parameters that have been used in the literature to characterize the relative magnitudes of the direction-dependent diffusion coefficients. The relative rates of diffusion in the straight and zigzag channel scan be simply characterized by the ratio D_y/D_x. The anisotropy parameter, A, which indexes the rate of diffusion in the z direction as a result of correlated motions in the x and y directions is defined as

$$A = (D_x + D_y)/2D_z \tag{9}$$

The randomization parameter, β, is defined as:

$$\beta = \frac{c^2/D_z}{a^2/D_x + b^2/D_y} \tag{10}$$

A value of unity for the β-parameter indicates that the basic assumption of Kärger's model is exactly obeyed, i.e., the probability of a sorbate to move in any one of four directions on reaching a channel intersection is the same. $\beta > 1$ indicates a tendency for the sorbate to continue in a channel of the same type, whereas $\beta < 1$ indicates a tendency to alternate between straight and zigzag channels.

2.3.3 Time-Correlation Functions. The velocity autocorrelation function is defined as

$$C_{vv}(t) = \frac{\langle \mathbf{v}(t)\cdot\mathbf{v}(0)\rangle}{\langle \mathbf{v}^2(0)\rangle} \tag{11}$$

and is related to the diffusion coefficient, D, by the relation:

$$D = (1/3) \int_0^\infty C_{vv}(t) dt \tag{12}$$

We have, however, not used the integral of the velocity

TABLE 2: Convergence Tests for CH_4 in Silicalite at Different Concentrations Measured in Sorbates Per Unit Cell[a]

				(kJ mol^{-1})		(10^{-8} m^{2}s^{-1})				diffusional			
conc	t_{prod} (ns)	t_{equil} (ns)	T (K)	$\langle U_{gh}\rangle$	$\langle U_{gg}\rangle$	D_x	D_y	D_z	D	n_x	n_y	n_z	n
2	5.3	5.3	305	−15.76	−0.09	0.62	0.60	0.19	0.43	0.89	1.05	0.83	0.99
	5.3	26.4	301	−15.75	−0.09	0.49	0.74	0.13	0.45	0.95	0.96	0.94	0.98
	26.4	26.4	305	−15.76	−0.09	0.49	0.56	0.15	0.39	0.95	1.02	0.91	0.99
8	5.3	5.3	305	−15.35	−0.49	0.49	0.63	0.23	0.43	0.93	0.99	0.81	0.96
	5.3	26.4	299	−15.37	−0.49	0.47	0.63	0.23	0.43	0.94	0.97	0.80	0.95
	26.4	26.4	298	−15.38	−0.49	0.48	0.59	0.20	0.41	0.93	0.99	0.83	0.90
12	5.3	5.3	303	−15.25	−0.78	0.36	0.51	0.15	0.34	0.91	0.94	0.84	0.92
	5.3	26.4	299	−15.26	−0.78	0.31	0.49	0.22	0.32	0.95	0.95	0.74	0.93
	26.4	26.4	299	−15.26	−0.79	0.30	0.47	0.16	0.31	0.95	0.96	0.82	0.94
16	5.3	5.3	300	−15.14	−1.04	0.22	0.36	0.19	0.23	0.89	0.96	0.68	0.92
	5.3	26.4	304	−15.12	−1.04	0.26	0.39	0.15	0.25	0.89	0.98	0.77	0.93
	52.8	26.4	317	−15.08	−1.04	0.20	0.41	0.12	0.24	0.95	0.96	0.81	0.95
24	5.3	5.3	291	−4.57	−0.98	0.15	0.14	0.15	0.11	0.74	0.98	0.55	0.89
	5.3	26.4	299	−4.51	−0.96	0.08	0.14	0.15	0.10	0.97	0.96	0.59	0.92
	52.8	26.4	298	−4.51	−0.97	0.08	0.14	0.09	0.09	0.94	0.95	0.69	0.93

[a] A time step of 5.3 fs was used for all the runs. Temperature scaling was carried out during the equilibration period, t_{equil}, and switched off during the production run of length, t_{prod}.

autocorrelation function to compute the diffusion coefficient since the relation using the mean square displacement as a function of time proves to be computationally more efficient. The directional analogues are defined as:

$$C_{v_x v_x}(t) = \frac{\langle \mathbf{v_x}(t)\cdot\mathbf{v}_x(0)\rangle}{\langle \mathbf{v}_x^2(0)\rangle} \tag{13}$$

$$C_{v_y v_y}(t) = \frac{\langle \mathbf{v_y}(t)\cdot\mathbf{v}_y(0)\rangle}{\langle \mathbf{v}_y^2(0)\rangle} \tag{14}$$

$$C_{v_z v_z}(t) = \frac{\langle \mathbf{v_z}(t)\cdot\mathbf{v}_z(0)\rangle}{\langle \mathbf{v}_z^2(0)\rangle} \tag{15}$$

The structure of the velocity autocorrelation function can provide information on the short and intermediate time dynamics of the system. The time, τ_n, at which $C_{vv}(t)$ first turns negative represents the average time at which the sorbate first encounters a repulsive barrier and is often closely related to the crossover time from ballistic to diffusional motion. The position of the first minimum in $C_{vv}(t)$ indicates the average time at which the sorbate is likely to reverse its direction of motion. As collisions with the wall and other sorbates increase, the correlation function decays to zero.

2.3.4 Convergence Tests. The statistical error in quantities such as the diffusion coefficient, which are both time-dependent and expressed in terms of a mean square deviation, are relatively much greater than for simple averages, such as the mean potential energy.[34,35] A detailed study of the error in the diffusion coefficient of sorbates in zeolites depends on the nature of the system and the underlying potential energy surface.[40] Since results reported in the literature vary significantly in terms of run lengths, equilibration protocols, and potential energy parametrizations, we have performed a fairly detailed set of convergence tests. The results for CH_4 in silicalite are summarized in Table 2. We have considered five different concentrations of 2, 8, 12, 16, and 24 atoms per unit cell as well as three different sets of equilibration times, t_{equil}, and production run lengths, t_{prod}, for each concentration. As expected, a simple statistical average such as the guest−host interaction energy, is very well converged even for the smallest concentration and run length. The sharp rise in $\langle U_{gh}\rangle$ on going from a concentration of 16/u.c. to 24/u.c. indicates that a concentration of 24 atoms per unit cell exceeds the maximum packing density for sorbates of this size.[33] Therefore, for CH_4 and Xe, we have not considered the results for concentrations above 16/u.c. Convergence of the D values with increasing equilibration and production times is much slower, as expected for a transport property, specially at the lowest concentration of 2/u.c. This is expected given the slow thermalization for very low sorbate concentrations in a rigid lattice in the NVE ensemble. A comparison with the results of Jost et al. who used an NVT ensemble with weak coupling to the thermal bath shows that the agreement between their results and ours is much better at higher concentrations.[8] On the basis of previous work,[26,27,40] we estimate an error of ±10% for the diffusion coefficients obtained from the longest runs. We also show the convergence behavior for the exponents, n_x, n_y, n_z, and n in the diffusional regime (see eqs 7 and 8). The convergence behavior of n_x, n_y, and n is more robust than that of n_z. As mentioned in the introduction, the motion in the z direction is a consequence of correlated motions along the x and y directions. The variation in the n_z values may therefore be due to two reasons: (i) slower diffusional motion along the z-axis and (ii) slow restoration of Fickian behavior in the very long-time limit. These points are discussed further in Section 3. It should be noted, however, that despite a relatively higher variation in n_z as compared to n_x and n_y, the n_z exponent is always lower than the exponents in the x and y direction.

Convergence tests, similar to those reported above for CH_4 and Xe, were carried out for the other four sorbates. The results reported here are for the longest run length simulation for each concentration. The corresponding simulation parameters are summarized in Table 3. On the basis of our convergence tests, we expect our diffusion coefficients to be correct to within ±10 to ±20% for the longest runs.

2.4 Instantaneous Normal-Mode Analysis. In this section, we first summarize those aspects of instantaneous normal mode (INM) analysis which have been found useful in understanding the short-time dynamics of simple sorbates in zeolites.[26,27] We then discuss the simple extensions necessary to study the effect of anisotropy of the confining potential on the INM spectrum.

An instantaneous normal-mode analysis is performed by expanding the potential energy function to second order in the displacement, $\boldsymbol{r}(t) - \boldsymbol{r}(0)$, where $\boldsymbol{r}(0)$ and $\boldsymbol{r}(t)$ are the configurations of the N-particle system at time $t = 0$ and at time t,

TABLE 3: Molecular Dynamics Simulation Parameters Used for Different Lennard−Jones Sorbates

sorbate	mass (amu)	time step (fs)	conc (sorbates/ u.c.)	t_{equil} (ns)	t_{prod} (ns)	T (K)	(kJ mol^{-1}) $\langle U_{gh}\rangle$	(kJ mol^{-1}) $\langle U_{gg}\rangle$
He	4	0.24	2	1.20	2.40	318	−2.40	0.002
			12	1.20	1.20	309	−2.31	0.02
			16	1.20	2.40	301	−2.33	0.03
			24	1.20	2.40	304	−2.31	0.06
Ne	20	0.48	2	4.80	19.20	299	−3.89	−0.007
			12	2.40	2.40	308	−3.76	−0.03
			16	2.40	4.80	299	−3.76	−0.04
			24	2.40	4.80	306	−3.64	−0.03
Ar	40	1.20	2	11.76	0.24	294	−11.47	−0.08
			12	6.00	6.00	296	−11.08	−0.60
			12	6.00	6.00	296	−11.08	−0.60
			16	6.00	12.00	285	−11.07	−0.82
			24	6.00	12.00	288	−10.95	−1.20
CH_4	16	5.30	2	26.4	26.4	305	−15.76	−0.09
			8	26.4	26.4	298	−15.38	−0.49
			12	26.4	26.4	299	−15.26	−0.79
			16	26.4	52.8	317	−15.08	−1.04
Xe	131	12.0	2	116.40	3.60	305	−27.97	−0.30
			12	60.00	60.0	304	−26.61	−2.93
			16	60.00	120.00	313	−26.35	−4.00

respectively. The short-time classical Hamiltonian can then be written as

$$H \approx \sum_{i=1}^{3N} \frac{1}{2}\left(\frac{dq_i}{dt}\right)^2 + V(\boldsymbol{r}(0)) - \boldsymbol{F}\cdot(\boldsymbol{q}(t) - \boldsymbol{q}(0)) + 0.5(\boldsymbol{q}(t) - \boldsymbol{q}(0))^T\cdot\boldsymbol{D}\cdot(\boldsymbol{q}(t) - \boldsymbol{q}(0)) \quad (16)$$

where the first and second derivative matrices of the potential, $\boldsymbol{F}$ and $\boldsymbol{D}$, respectively, are constructed with respect to the mass-weighted coordinates, **q**. The Hessian matrix can be diagonalized to give the eigenvalues, $\{\omega_i^2,\ i = 1,\ 3N\}$, and eigenvectors $\boldsymbol{U}(\boldsymbol{r}(0))$. The eigenvalues correspond to the squares of the normal-mode frequencies and may be positive or negative corresponding to real and imaginary frequencies, respectively. Conventionally, the imaginary branch is depicted on the negative frequency axis.

The INM spectrum or the normalized INM density of states is obtained by averaging the INM frequencies over a set of configurations sampled from the equilibrium distribution in any ensemble. Mathematically, it may be represented as

$$\rho(\omega) = \langle(1/3N)\sum_{k=1}^{3N}\delta(\omega - \omega_k(\mathrm{r}))\rangle \quad (17)$$

The fraction of imaginary modes, F_i, indicates the extent to which the system samples regions of negative curvature, including barrier and shoulder regions of the PES. Previous studies indicate that F_i is generally correlated with the magnitude of the self-diffusion coefficient. The Einstein frequency, ω_E, is defined as: $\omega_E^2 = \int \omega^2\rho(\omega)d\omega$ where $\rho(\omega)$ is the normalized INM spectrum. The Einstein frequency is a measure of the average force constant, $\langle V''\rangle/3N$, of the system.

For a classical system, it is possible to obtain an approximation to the short-time dynamics in terms of the kinematics of the normal mode coordinates. On the basis of the time evolution of the classical normal modes, it has been shown that the velocity autocorrelation function is given by:

$$C_{vv}(t) = \int_{\mathrm{real}}\rho(\omega)\cos(\omega t)d\omega \quad (18)$$

where the integration is restricted to only the real branch of the INM spectrum. For simple liquids and for rare gases in zeolites, the short time behavior of the translational autocorrelation function is well reproduced by the above formula provided F_i is not too large.

To define the components of the INM spectrum along the three Cartesian directions, an eigenvector representing the kth mode associated with some configuration is denoted by

$$\psi_k = \sum_{j=1}^{N}\sum_{\beta} U_{k,j\beta}|\xi_{j\beta}\rangle \quad (19)$$

where $\xi_{j\beta}$ is the mass-weighted displacement of the jth atom in the β-direction with $\beta = x$, y, or z. In the case of orthorhombic zeolites, projections along Cartesian directions are equivalent to projections along the crystallographic axes. We wish to separate the INM density of states into the direction-dependent densities of states $\rho^\beta(\omega)$ such that $\rho^\beta(\omega)$ indicates the probability of finding a mode with frequency ω with a projection in the β-direction. Following earlier approaches for computing translational and rotational components of INMs in molecular liquids, we define the projection matrix

$$P_{kl}^\beta = \langle\psi_k|\hat{p}_\beta\hat{p}_\beta|\psi_l\rangle \quad (20)$$

where

$$\hat{p}_\beta|\psi_l\rangle = \sum_{j=1}^{N} U_{l,j\beta}\xi_{j\beta} \quad (21)$$

and the diagonal elements of the projection matrix are

$$P_{kk}^\beta = \sum_{j=1}^{N} U_{k,j\beta}^2 \quad (22)$$

Since $P_{kk}^x + P_{kk}^y + P_{kk}^z = 1$, we can write

$$\rho(\omega) = \rho^x(\omega) + \rho^y(\omega) + \rho^z(\omega) \quad (23)$$

where

$$\rho^\beta(\omega) = \langle(1/3N)\sum_{k=1}^{3N} P_{kk}^\beta\delta(\omega - \omega_k(\boldsymbol{r}))\rangle \quad (24)$$

Each of the direction-dependent densities of states will have a fraction of imaginary modes, F_i and given our definition, $F_i = F_{ix} + F_{iy} + F_{iz}$.

3. Results and Discussion

3.1 Diffusional and Ballistic Regimes. The separation between the ballistic and diffusional regimes is most clearly shown in log−log plots of the mean square displacement against time. As an illustration, Figure 2 compares the direction-dependent mean square displacements, $\Delta^2x(t)$, $\Delta^2y(t)$, and $\Delta^2z(t)$, against time for CH_4 in silicalite. The slopes for all three curves in the ballistic region from 0 to approximately 0.5 ps are very close to 2. The transition to the diffusional regime is marked by a crossover period rather than a sharp crossover time, τ_c. More interestingly, the slopes in the diffusional regime are close to unity but are by no means identical—the n_x and n_y values are 0.95 and 0.96, respectively, while n_z is 0.82. The net mean square displacement, $\Delta^2\boldsymbol{r}(t)$ grows as $t^{0.94}$. Thus, sorbate motion along the z direction, corresponding to the c-axis of the unit cell, is distinctly subdiffusional. From Table 4, it can be seen that this subdiffusional behavior for the z-displacement is present for all the sorbates studied here, although it is least pronounced

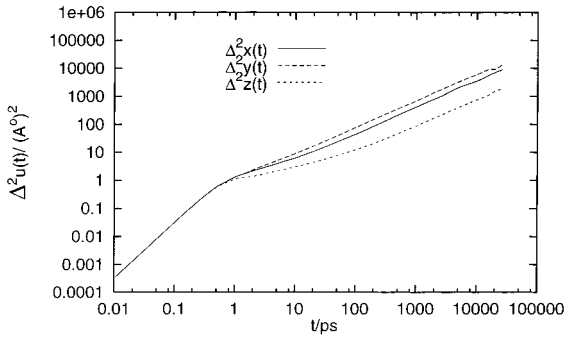

Figure 2. Log_{10}−log plot of mean square displacements in the *x*, *y*, and *z* directions as a function of time for CH_4 in silicalite at 300 K and a concentration of 12 particles per unit cell.

TABLE 4: The Exponent of the Time Dependence of the Mean Square Displacement in the Ballistic and Diffusional Regimes for Different Lennard−Jones Sorbates in Silicalite[a]

	conc	ballistic				diffusional			
sorbate	(sorbates/u.c.)	n_x	n_y	n_z	n	n_x	n_y	n_z	n
He	2	1.93	1.94	1.92	1.93	0.99	0.93	0.93	0.96
	12	1.91	1.92	1.90	1.91	0.98	1.02	0.87	0.99
	16	1.91	1.92	1.90	1.91	1.00	1.03	0.93	1.01
	24	1.90	1.90	1.89	1.90	1.01	1.00	0.90	1.00
Ne	2	1.91	1.91	1.90	1.91	0.98	1.01	0.81	1.00
	12	1.93	1.94	1.93	1.90	0.96	1.09	0.83	1.02
	16	1.93	1.93	1.92	1.93	1.00	0.95	0.89	0.96
	24	1.91	1.91	1.91	1.91	0.94	0.99	0.90	0.96
Ar	2	1.96	1.96	1.95	1.96	0.99	1.02	0.79	1.00
	12	1.94	1.94	1.94	1.94	0.92	0.96	0.73	0.92
	16	1.93	1.93	1.93	1.93	0.93	0.98	0.78	0.94
	24	1.90	1.89	1.89	1.90	0.88	0.93	0.70	0.87
CH_4	2	1.95	1.95	1.93	1.94	0.95	1.02	0.91	0.99
	8	1.93	1.93	1.92	1.93	0.93	0.99	0.83	0.90
	12	1.90	1.90	1.90	1.90	0.95	0.96	0.82	0.94
	16	1.90	1.90	1.90	1.90	0.95	0.96	0.81	0.95
Xe	2	1.94	1.93	1.91	1.93	0.91	0.93	0.76	0.91
	12	1.89	1.89	1.89	1.89	0.92	0.97	0.78	0.94
	16	1.87	1.86	1.87	1.87	0.89	1.01	0.76	0.98

[a] The exponents n_x, n_y, n_z and n corresponds to the $\Delta^2x(t)$, $\Delta^2y(t)$, $\Delta^2z(t)$, and $\Delta^2r(t)$ displacements, respectively. Simulation parameters, as well as the mean temperature and potential energy, are given in Table 3.

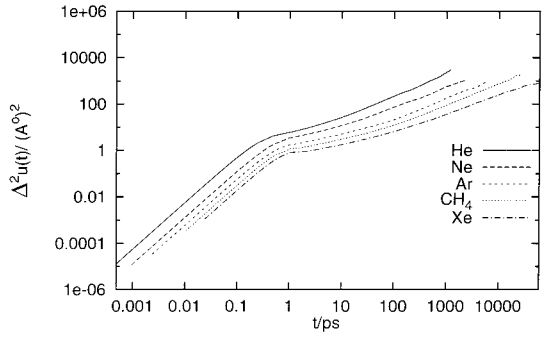

Figure 3. Log_{10}−log plot comparing mean square displacements in the *z* direction, $\Delta^2z(t)$, versus time for different Lennard−Jones sorbates in silicalite at 300 K and a concentration of 12 particles per unit cell.

for helium. Figure 3 also illustrates this by comparing the mean square displacements in the *z* direction as a function of time for all the five sorbates studied here. The general result that emerges from the results in Table IV is that the relative values of n_x, n_y, and n_z are influenced by the size, polarizability, and concentration of the sorbate. At a given concentration, the smaller and less polarizable the sorbate, the smaller the anisotropy and subdiffusional character manifested by the n_x, n_y, and n_z exponents. For a given sorbate, increasing the concentration promotes subdiffusional behavior along the *z* direction, relative to the other two directions. Exceptions to these trends do arise which must be accounted for by a more detailed analysis of factors influencing diffusion. For example, n_z values for CH_4 are somewhat higher than the corresponding values for Ar. From Table 1, it can be seen that ϵ_{SS} is very similar for both sorbates, but σ_{SS} is about 10% greater for CH_4. It may be conjectured that the larger sorbate is forced to occupy positions close to the channel centers and therefore may show different diffusional behavior. Other factors that may play a role are the number of lowest energy sorption sites available for a sorbate of given size.

TABLE 5: Ballistic to Diffusional Crossover Times (in ps) for Lennard−Jones Sorbates in Silicalite at a Temperature of 300 K and Concentration of 12 Particles Per Unit Cell

sorbate	τ_{cx}	τ_{cy}	τ_{cz}	τ_c
He	0.29	0.31	0.11	0.23
Ne	0.40	0.28	0.21	0.26
Ar	0.29	0.31	0.24	0.26
CH_4	0.24	0.37	0.23	0.26
Xe	0.20	0.35	0.18	0.21

Since the greater tendency to subdiffusional behavior along the *z* direction is a very distinct feature of diffusional anisotropy that emerges from our study, it is worthwhile to examine it more carefully. Previous studies of the time dependence of the MSDs of sorbates in zeolites have not considered anisotropic effects. The diffusion of CH_4 in silicalite has, however, been reported as being subdiffusional with an exponent of 0.78 at a temperature of 298 K.[36] We find, however, that the exponent for the total MSD is 0.94. The differences between their study and ours may stem from different potential energy surfaces as well as much shorter run lengths (0.2 ns as opposed to 2.6 ns). Our study finds distinctly subdiffusional behavior only along the *z* direction. The n_z exponent for different run lengths is fairly similar and therefore is unlikely to be an artifact of a simulation that is too short. It would therefore appear that this type of subdiffusional motion is a consequence of the correlated nature of diffusion along the *z*-axis which can take place only if the particle alternately diffuses through straight and zigzag channel segments. However, the geometry of the channel network is clearly not the only determining factor since the very small, light, and weakly bound helium atom does not display such pronounced diffusional anisotropy. It is also clear that the subdiffusional behavior is more pronounced at higher concentrations indicating that avoided crossings of sorbates in the *z* direction may play a role, as in the case of single-file diffusion. It would appear therefore that a combination of the potential energy landscape within a channel, the packing density as well as the geometrical connectivity is necessary to produce this subdiffusional behavior. On the basis of this, one can predict that similar direction-dependent subdiffusional behavior will be present in other two-dimensional networked channel zeolites, such as ZSM-11, and the effect will be attenuated with increasing temperature and accentuated by increasing concentration. In future work, it will be of interest to examine if there is a slow approach to Fickian behavior in the long-time limit, as has been suggested in the case of single-file systems.[42]

The crossover time from ballistic to diffusional motion has been computed as the point of intersection of the straight line fits to the MSDs in the two regions. The results, for 12 particles per unit cell, are given in Table 5. The crossover times are found to be fairly similar for all the systems and the most notable

TABLE 6: Diffusion Coefficients of Different Lennard−Jones Sorbates in Silicalite at a Temperature of 300 K at Different Concentrations

sorbate	conc (sorbates/u.c.)	(kJ mol^{-1})		(10^{-8} m^2 s^{-1})						
		U_{gg}	U_{gh}	D_x	D_y	D_z	D	A	β	D_y/D_x
He	2	−2.40	0.002	7.08	11.21	1.65	6.61	5.54	1.18	1.58
	12	−2.31	0.02	6.28	7.22	1.97	5.10	3.43	0.76	1.15
	16	−2.33	0.03	5.19	6.03	1.55	4.21	3.62	0.81	1.16
	24	−2.31	0.06	4.29	5.74	1.57	3.13	3.19	0.70	1.34
Ne	2	−3.89	−0.007	2.29	2.55	1.02	1.86	2.37	0.53	1.11
	12	−3.76	−0.03	1.89	1.60	0.80	1.33	2.18	0.49	0.85
	16	−3.76	−0.03	1.38	2.07	0.58	1.32	2.97	0.64	1.50
	24	−3.64	−0.03	1.32	1.36	0.45	1.03	2.98	0.67	1.03
Ar	2	−11.47	−0.09	0.76	0.94	0.38	0.65	2.24	0.50	1.24
	12	−11.08	−0.60	0.66	0.73	0.31	0.55	2.24	0.50	1.11
	16	−11.07	−0.82	0.44	0.47	0.26	0.37	1.75	0.39	1.07
	24	−10.95	−1.20	0.22	0.19	0.22	0.19	0.93	0.21	0.86
CH_4	2	−15.76	−0.09	0.49	0.56	0.15	0.39	3.50	0.78	1.14
	8	−15.38	−0.49	0.48	0.59	0.20	0.41	2.68	0.60	1.23
	12	−15.27	−0.79	0.30	0.47	0.16	0.31	2.41	0.51	1.57
	16	−15.08	−1.04	0.20	0.41	0.12	0.24	2.54	0.50	2.05
Xe	2	−27.97	−0.30	0.11	0.16	0.05	0.10	2.70	0.59	1.45
	12	−26.61	−2.93	0.14	0.29	0.12	0.17	1.79	0.35	2.07
	16	−26.35	−4.00	0.06	0.18	0.05	0.09	2.40	0.40	3.00

feature is that the crossover time for the MSD in the *z* direction is distinctly lower than the crossover times in the other two directions. There is, however, some ambiguity in the exact location of τ_c because of the extended nature of the crossover region. An examination of Figure 2 also indicates that the above method of locating τ_c will generally result in values that are lower than the time at which the MSD begins to show a deviation from ballistic behavior on a log−log plot. Intuitively, our results for a reduced value for τ_{cz}, as compared to τ_{cx} or τ_{cy}, do appear to be reasonable since the range of ballistic motion in the *z* direction is strongly confined by the channel walls.

Table 6 shows the direction-dependent diffusion coefficients as well as the anisotropy parameter, A, the randomization parameter, β, and the ratio D_y/D_x. As expected, the diffusion coefficients decrease with increasing binding energy and size of the sorbate. The D_y/D_x ratio is most sensitive to the specific nature of the sorbate. This must reflect differences in the straight and zigzag channel architecture experienced by the different diffusing particles. Increasing concentration results in lowering the diffusion coefficients, as well as the anisotropy and randomization parameters. The assumption of complete randomization which underlies eq 1 appears to be most closely obeyed by the He sorbate which is entirely expected given the small size, weak binding, and high diffusion coefficients for this system. For all concentrations of helium in silicalite, $\beta \approx 1$ and $A \approx 4$. The simple random walk model of Kärger predicts $\beta = 1$ and $A > 4.4$. Clearly, the motion of the helium atoms is very rapidly randomized in the channels so that at the channel intersection the probability of moving in any four of the available channel segments is essentially equal. The other four sorbates, on the other hand, have β values very close to 0.5, indicating a propensity for the sorbates to alternate between straight and zigzag channels on reaching an intersection presumably due to greater influence of the local nature of the potential energy surface. The anisotropy parameter, A, is approximately 2 for the larger sorbates, instead of ≈ 4 for helium. The results for β and A are consistent with our results for the exponent of the time dependence which also indicate that helium is clearly a sorbate that closely obeys the assumptions underlying the simple random walk model.

It is important at this point to make an explicit comparison with previous work on diffusional anisotropy. Only two Lennard−Jones sorbates, Xe and CH_4, have been studied from the point of view of understanding diffusional anisotropy in silicalite. Our potential energy parameters for CH_4 are identical to those used by Jost et al. Their results are $D_x = 0.5$, $D_y = 0.6$, $D_z = 0.1$, and $D = 0.4$ in units of 10^{-8} m^2 s^{-1}, which may be compared with our results in Table 6. The agreement is reasonable given that the values quoted from ref 8 have been read of the graph and therefore are approximate. Results for xenon show poorer agreement partly because of small differences in potential energy parameters. In general, we find that D_z values are overestimated and the β parameters underestimated when compared with previous work. This may be due to differences in run lengths. A more important reason, in our opinion, is that we have allowed the exponent of the time dependence of the MSD to deviate from unity, whereas in past work, a linear dependence on time has been assumed.

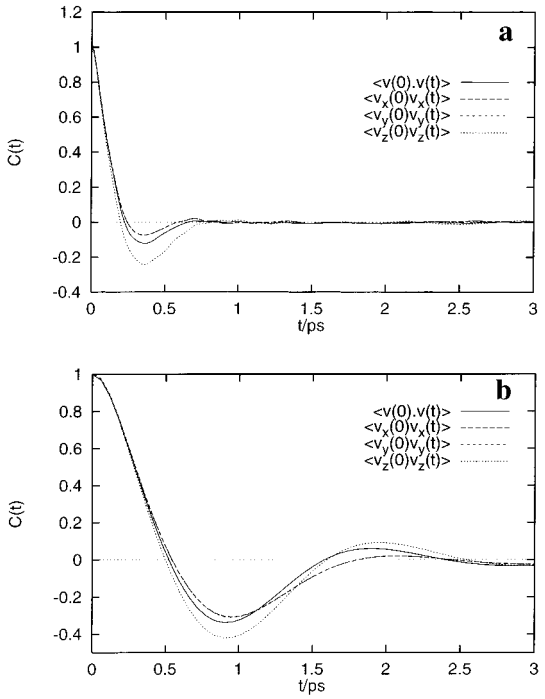

Figure 4. Short-time behavior of time correlation functions for (a) xenon and (b) neon in silicalite at 300 K and a concentration of 12 particles per unit cell.

3.2 The Velocity Autocorrelation Function. We have looked at the short-time behavior of the velocity autocorrelation function, $C_{vv}(t)$, and its directional counterparts, $C_{v_xv_x}(t)$, $C_{v_yv_y}(t)$, and $C_{v_zv_z}(t)$. Figure 4 shows the four correlation functions for neon and xenon in silicalite. $C_{v_xv_x}(t)$ and $C_{v_yv_y}(t)$ are indistinguishable on the scale of the plots. $C_{v_zv_z}(t)$ differs from its counterparts in the *x* and *y* directions in having a much deeper first minimum. In the case of xenon, $C_{v_zv_z}(t)$ also has a pronounced second maximum (also seen in methane and argon) which is absent for helium and neon. All the four velocity autocorrelation functions for each system are almost identical until a time τ_n when they first turn negative. While the location of the first minimum occurs for smaller times for the more mobile sorbates, the location of τ_n for four larger sorbates is between 0.4 and 0.5 ps. Earlier work on diffusion in faujasite indicated that τ_n is strongly correlated with the ballistic to diffusional crossover time, τ_c.[27] In silicalite, however, τ_n is found to be significantly larger than the τ_c values which lie between 0.2 and 0.4 ps.

3.3 Instantaneous Normal-Mode Analysis. Table 7 summarizes the key features of the INM spectra. As expected on

TABLE 7: Key Features of the Instantaneous Normal Mode Spectra for Lennard−Jones Sorbates in Silicalite at a Concentration of 12 Particles Per Unit Cell and a Temperature of 300 K

sorbate	F_i	F_{ix}	F_{iy}	F_{iz}	ω_E (cm^{-1})
He	0.50	0.16	0.16	0.17	67.7
Ne	0.46	0.15	0.15	0.15	41.3
Ar	0.39	0.13	0.13	0.13	34.4
CH_4	0.33	0.12	0.11	0.11	25.4
Xe	0.28	0.10	0.09	0.09	22.9

the basis of previous studies, there is a strong correlation between the diffusion coefficient, D, the fraction of imaginary modes, F_i, and the Einstein frequency, ω_E. The fraction of imaginary modes for the projections of the INM density of states on the x, y, and z axes is essentially identical. This is consistent with the isotropy in the short-time dynamics that is displayed by the velocity autocorrelation functions. On the basis of our previous work, the time scales for which the INM approach can be expected to be useful can be estimated from the value of τ_n, the time at which the velocity autocorrelation function first turns negative. Since this is of the order of 0.5 ps, and at thermal velocities at 300 K corresponds to distances of a few angströms, it is not surprising that the INM spectra are not sensitive to the geometrical connectivity of the silicalite lattice which manifests its anisotropy over longer length scales. Moreover, the INM spectrum can be thought of as displaying the local curvature of the PES as sampled by the system. A diffusional property, such as the levitation effect, which is closely connected with the curvature distribution of the potential will be mirrored by changes in the INM spectrum. Geometrical correlations in the principal components of the diffusional tensor are not, however, expected to have a close connection with the PES. The anomalous levitation peak for sorbates in silicalite has been observed for sorbates in the size range from 1.5 to 2.2 Å; as discussed in section 2.2, we believe the Kiselev potential energy parametrization to be somewhat problematic in this size regime, and we have therefore not studied the levitation effect in this zeolite.

4. Conclusions

In this work, we have studied the anisotropy in diffusional and related dynamical properties for five spherical sorbates of varying size and polarizability in silicalite. Helium, the smallest and most weakly bound sorbate, complies most closely with the behavior expected on the basis of the simple random walk model of Kärger with a randomization parameter close to 1 and an anisotropy parameter close to 4. The larger and more strongly bound sorbates (Ne, Ar, CH_4, and Xe) show significant deviations from this model. The diffusion of these particles along the z direction is distinctly subdiffusional with the mean square displacement growing as $\approx t^{0.8}$. The randomization parameters for all these systems are close to 0.5, and the anisotropy parameters are all close to 2. The relative rates of diffusion along the straight and zigzag channels are more sensitive to the nature of the sorbate than the anisotropy and randomization parameters. For all five sorbates, the subdiffusional behavior along the z direction as well as deviations from the predictions of the random walk model are more pronounced at higher concentrations. The subdiffusional motion along the z direction appears to be a consequence of a combination of factors: (i) the geometrical connectivity of the silicalite channel network, (ii) the nature of the potential energy landscape seen by a sorbate located within the channel spaces, and (iii) the packing density. On the basis of our results, one would expect such subdiffusional behavior in specific directions for sorbates in other zeolites which can display geometrical correlations in diffusional behavior, e.g., ZSM-11 and chabazite. The PES dependence would imply that such subdiffusional behavior would become less prominent with increasing temperature. The anisotropy in the short-time dynamics has been examined by studying the velocity autocorrelation functions and the instantaneous normal mode spectra. For very short-times of less than 0.5 ps, the velocity autocorrelation function and its directional analogues are virtually identical but divergences are seen by times of the order of 1 ps. The motion along the z direction is clearly more correlated than along the x or y directions. The instantaneous normal mode spectra show the expected correlation between the diffusion coefficient, the Einstein frequency, and the fraction of imaginary modes. There is no significant anisotropy in the INM spectra which is consistent with the behavior of the velocity autocorrelation functions for short time scales. Our results suggest that there are several aspects to diffusional anisotropy, in addition to the relative magnitudes of the direction-dependent diffusion constants, which may be worth exploring further. These include the extent of subdiffusional behavior and the short-time dynamics. The qualitative difference in behavior of helium and xenon as sorbates in silicalite may be of interest experimentally since ^{129}XeNMR spectroscopy is widely used, and ^{3}He NMR has been suggested as a probe in porous media.[41] One can also predict that similar direction-dependent subdiffusional behavior will be present in other two-dimensional networked channel zeolites, such as ZSM-11 and gismondine, and that the effect will be attenuated with increasing temperature and accentuated by increasing concentration. In future work, it will also be of interest to examine if there is a slow approach to Fickian behavior in the long-time limit for such systems.

Acknowledgment. This work was supported by the Indian National Science Academy (INSA) and the Council for Scientific and Industrial Research (CSIR).

References and Notes

(1) Barrer, R. M. *Zeolites and Clay Minerals as Sorbents and Molecular Sieves*; Academic Press: New York, 1978.
(2) Breck, D. W. *Zeolite Molecular Sieves*; Wiley-Interscience: New York, 1974.
(3) Demontis, P.; Suffriti, G. B. *Chem. Rev.* **1997**, *97*, 2845.
(4) Cracknell, R. F.; Gubbins, K. E.; Maddox, M.; Nicholson, D. *Acc. Chem. Res.* **1995**, *28*, 281.
(5) Kärger, J.; Ruthven, D. M. *Diffusion in Zeolites and Other Microporous Solids*; Wiley: New York, 1992.
(6) Kärger, J. *J. Phys. Chem.* **1991**, *95*, 5558.
(7) Maginn, E. J.; Bell, A. T.; Theodorou, D. N. *J. Phys. Chem.* **1996**, *100*, 7155.
(8) Jost, S.; Bär, N.-K.; Fritzsche, S.; Haberlandt, R.; Kärger, J. *J. Phys. Chem.* **1998**, *102*, 6375.
(9) Kärger, J.; Demontis, P.; Suffriti, G. B.; Tilocca, A. *J. Chem. Phys.* **1999**, *110*, 1163.
(10) Jousse, F.; Auerbach, S. M.; Vercauteren, D. P. *J. Chem. Phys.* **2000**, *112*, 1531.
(11) Hahn, K.; Kärger, J. *J. Phys. Chem.* **1996**, *100*, 316.
(12) Kukla, V.; Kornatowski, J.; Demuth, D.; Girnus, I.; Pfeifer, H.; Rees, L. V. C.; Schunk, S.; Unger, K. K.; Kärger, J. *Science* **1996**, *272*, 702.
(13) Scholl, D. S.; Fichthorn, K. A. *J. Chem. Phys.* **1997**, *107*, 4384.
(14) Hoogenboom, J. P.; Tepper, H. L.; van der Vegt, N. F. A.; Briels, W. J. *J. Chem. Phys.* **2000**, *113*, 6875.
(15) Tepper, H. L.; Hoogenboom, J. P.; van der Vegt, N. F. A.; Briels, W. J. *J. Chem. Phys.* **1999**, *110*, 11511.
(16) Derouane, E. G.; Andre, J.-M.; Lucas, A. A. *Chem. Phys. Lett.* **1987**, *137*, 336.
(17) Yashonath, S.; Santikary, P. *J. Phys. Chem.* **1994**, *98*, 6368.
(18) Yashonath, S.; Bandhopadhyay, S. *Chem. Phys. Lett.* **1994**, *228*, 284.
(19) Bandhopadhyay, S.; Yashonath, S. *J. Phys. Chem.* **1995**, *99*, 4286.

(20) Wang, Q.; Challa, S. R.; Scholl, D. S.; Johnson, J. K. *Phys. Rev. Lett.* **1999**, *82*, 956.
(21) Stratt, R. M. *Acc. Chem. Res.* **1995**, *28*, 201.
(22) Buchner, M.; Ladanyi, B. M.; Stratt, R. M. *J. Chem. Phys.* **1992**, *97*, 8522.
(23) Stratt, R. M.; Marconelli, M. *J. Phys. Chem.* **1996**, *100*, 12981.
(24) Chakravarty, C. *J. Phys. Chem.* **1997**, *100*, 11878.
(25) Chakravarty, C.; Thiruvengadaravi, K. V. Proceedings of the conference on *Frontiers in Materials Modelling and Design*; 20−23 August '96, Kalpakkam, Springer-Verlag, 1997.
(26) Mehra, V.; Basra, R.; Khanna, M.; Chakravarty, C. *J. Phys. Chem. B* **1999**, *14*, 2740.
(27) Kar, S.; Chakravarty, C. *J. Phys. Chem. B* **2000**, *104*, 709.
(28) Lermer, H.; Draeger, M.; Steffen, J.; Unger, K. K. *Zeolites* **1985**, *5*, 131.
(29) Olson, D. H.; Kokotailo, G. T.; Lawton, S. L.; Meier, W. M. *J. Phys. Chem.* **1981**, *85*, 2238.
(30) Bezus, A. G.; Kiselev, A. V.; Lopatkin, A. A.; Pham Quang Du *J. Chem. Soc., Faraday Trans. 2*, **1978**, *74*, 367.
(31) Kiselev, A. V.; Pham Quang Du *J. Chem. Soc., Faraday Trans. 2*, **1981**, *77*, 1.
(32) Kiselev, A. V.; Lopatkin, A. A.; Shulga, A. A. *Zeolites* **1985**, *5*, 261.
(33) El Amrani, S.; Vigné-Maeder, F.; Bigot, B. *J. Phys. Chem.* **1992**, *96*, 9417.
(34) Allen, M. P.; Tildesley, D. J. *Computer Simulation of Liquids*; Clarendon Press: Oxford, 1987.
(35) Frenkel, D.; Smit, B. *Understanding Molecular Simulation: From Algorithms to Applications*; Academic Press: USA, 1996.
(36) Ghosh, M.; Ananthakrishna, G.; Yashonath, S.; Demontis, P.; Suffriti, G. *J. Phys. Chem.* **1994**, *98*, 9354.
(37) Demontis, P.; Suffriti, G. B.; Fois, E. S.; Quartieri, S. *J. Phys. Chem.* **1992**, *96*, 1482.
(38) Demontis, P.; Suffriti, G. B.; Quartieri, S.; Fois, E. S.; Gamba, A. *J. Phys. Chem.* **1988**, *92*, 867.
(39) Fritzsche, S.; Haberlandt, R.; Kaerger, J.; Pfeifer, H.; Wolfsberg, M. *Chem. Phys. Lett.* **1990**, *171*, 109.
(40) Chitra, R.; Yashonath, S. *J. Phys. Chem.* **1997**, *101*, 5437.
(41) Saunders, M.; Jimenez-Vazquez, H. A.; Cross, R. J.; Billups, W. E.; Gesenberg, C.; Gonzalez, A.; Luo, W.; Haddon, R. C.; Diederich, F.; Hermann, A. *J. Am. Chem. Soc.* **1995**, *117*, 9305.
(42) Nelson, P. H.; Auerbach, S. M. *J. Chem. Phys.* **1999**, *110*, 9235.